PNAS RESEARCH ARTICLE | MEDICAL SCIENCES

FLASH X-ray spares intestinal crypts from pyroptosis initiated by cGAS-STING activation upon radioimmunotherapy

Xiaolin Shi[a,1], Yiwei Yang[b,1], Wei Zhang[c,1], Jianxin Wang[b,d,1], Dexin Xiao[b], Huangge Ren[a], Tingting Wang[e,f], Feng Gao[e,f], Zhen Liu[g], Kui Zhou[b], Peng Li[b], Zheng Zhou[b], Peng Zhang[b], Xuming Shen[b], Yu Liu[b], Jianheng Zhao[b], Zhongmin Wang[h], Fenju Liu[a], Chunlin Shao[i], Dai Wu[b,f,2], and Haowen Zhang[a,i,2]

Edited by James Cleaver, University of California San Francisco Medical Center at Parnassus, San Francisco, CA; received May 17, 2022; accepted September 11, 2022

DNA-damaging treatments such as radiotherapy (RT) have become promising to improve the efficacy of immune checkpoint inhibitors by enhancing tumor immunogenicity. However, accompanying treatment-related detrimental events in normal tissues have posed a major obstacle to radioimmunotherapy and present new challenges to the dose delivery mode of clinical RT. In the present study, ultrahigh dose rate FLASH X-ray irradiation was applied to counteract the intestinal toxicity in the radioimmunotherapy. In the context of programmed cell death ligand-1 (PD-L1) blockade, FLASH X-ray minimized mouse enteritis by alleviating $CD8^+$ T cell-mediated deleterious immune response compared with conventional dose rate (CONV) irradiation. Mechanistically, FLASH irradiation was less efficient than CONV X-ray in eliciting cytoplasmic double-stranded DNA (dsDNA) and in activating cyclic GMP-AMP synthase (cGAS) in the intestinal crypts, resulting in the suppression of the cascade feedback consisting of $CD8^+$ T cell chemotaxis and gasdermin E-mediated intestinal pyroptosis in the case of PD-L1 blocking. Meanwhile, FLASH X-ray was as competent as CONV RT in boosting the antitumor immune response initiated by cGAS activation and achieved equal tumor control in metastasis burdens when combined with anti–PD-L1 administration. Together, the present study revealed an encouraging protective effect of FLASH X-ray upon the normal tissue without compromising the systemic antitumor response when combined with immunological checkpoint inhibitors, providing the rationale for testing this combination as a clinical application in radioimmunotherapy.

FLASH X-ray | pyroptosis | cGAS-STING pathway | radioimmunotherapy | PD-L1

Significance

Tumor immunotherapy synergized with radiotherapy (RT) has become promising for eradicating multiple advanced tumors. However, accompanying treatment-related detrimental events in normal tissues has been the dark side of the combination regimen, for patients potentially amenable for radioimmunotherapy. This study identifies that ultrahigh dose rate (110 to 120 Gy/s) FLASH X-ray irradiation can reduce intestinal pyroptosis and thus counteracts the intestinal toxicity induced by conventional dose rate (CONV) irradiation in the context of programmed cell death ligand-1 (PD-L1) blockade. Meanwhile, FLASH X-ray achieves comparable efficacy with CONV RT in both primary and abscopal tumor control when combined with anti–PD-L1 administration, thus widening the therapeutic window of tumor radioimmunotherapy and potentially contributing to enhancing the popularity of this combination regimen.

Due to the encouraging success of tumor immunotherapy toward various malignancies, tumor immunology based on checkpoint blockade has opened up another era of clinical oncology (1–3). Recently, antibodies against programmed cell death-1 (PD-1) or programmed cell death ligand-1 (PD-L1) have been widely used in clinical cancer treatments, with ∼3,700 active clinical trials worldwide as of September 2020 testing anti–PD-1/PD-L1 monoclonal antibodies, representing a nearly threefold increase since September 2017 (4). Nonetheless, response rates achievable with anti–PD-1/PD-L1 inhibitors as a standalone treatment remain extremely modest (5), with a current "ceiling" lower than 40% (6). The leading cause of individuals with poor efficacy notably contributes to the absence of intratumoral T cell infiltration (5). As a result, other combination strategies that may improve the intratumoral T cell response and efficacy of immune checkpoint inhibitors are being extensively researched (7, 8). Take China, for example; in the past 2 y, the patient recruitment rate in anti–PD-1/PD-L1 combination trials rose by around one-fifth, while the recruitment rate in anti–PD-1/PD-L1 monotherapy trials saw a decrease of two-fifths (4).

Recently, DNA damage-induced tumor immunogenicity has emerged as a critical determinant of the antitumor immune response, as the DNA damage response deficiency-caused intrinsic genomic instability within tumor cells could be further amplified by DNA-damaging treatments (5, 9). DNA damage could generate DNA fragments that are recognized by cytoplasmic nucleic acid sensor cyclic GMP-AMP synthase (cGAS), which further promotes the expression of type I interferon (IFN) enhancing T cell chemotaxis and antitumor immune infiltration (10). Therefore, DNA damage-targeted therapies are considered to be promising to make up for the limitations of anti–PD-1/PD-L1 as a standalone treatment, thereby dramatically augmenting antitumor immunity (11, 12). However, accompanying treatment-related detrimental inflammatory response in normal tissues has become the dark side of combination regimens, mediating robust immunostimulatory effects. Taking the combination of radiotherapy (RT) and anti–PD-1/PD-L1 inhibitors as an example, the overall incidence of treatment-related adverse responses in the combined treatment was ∼90% for all-grade

Author contributions: Y.Y., J.W., F.G., C.S., D.W., and H.Z. designed research; X. Shi, Y.Y., W.Z., J.W., D.X., H.R., T.W., F.G., Z.L., K.Z., P.L., Z.Z., P.Z., X. Shen, Y.L., J.Z., Z.W., F.L., and H.Z. performed research; X. Shi, Y.Y., W.Z., H.R., and H.Z. analyzed data; and X. Shi, Y.Y., D.W., and H.Z. wrote the paper.

The authors declare no competing interest.

This article is a PNAS Direct Submission.

Copyright © 2022 the Author(s). Published by PNAS. This article is distributed under Creative Commons Attribution-NonCommercial-NoDerivatives License 4.0 (CC BY-NC-ND).

[1]X. Shi, Y.Y., W.Z., and J.W. contributed equally to this work.

[2]To whom correspondence may be addressed. Email: wudai04@caep.cn or hwzhang@suda.edu.cn.

This article contains supporting information online at http://www.pnas.org/lookup/suppl/doi:10.1073/pnas.2208506119/-/DCSupplemental.

Published October 18, 2022.

and more than 12% for grade 3 or higher (13). In the pembrolizumab in muscle-invasive/metastatic bladder cancer (PLUMMB) trial (NCT02560636), combining pembrolizumab (anti–PD-1 antibody) that blocks the PD-1/PD-L1 signal and hypofractionated RT (36 Gy in six fractions) in bladder cancer patients, two of the five patients developed grade 3 urinary toxicity, while one patient developed a grade 4 rectal perforation due to the trial treatment (14). These severe immune-related adverse events posed a major obstacle to the combination regimen for patients potentially amenable for radioimmunotherapy, limiting the radiation dose-dependent efficacy (15). Therefore, the implementation of radioimmunotherapy requires strategies to limit toxicity, and any approach that enhances normal tissue tolerance upon the integration regimen would dramatically widen the therapeutic window to achieve enhanced tumor control.

Intriguingly, in 2014, Favaudon et al. (16) demonstrated that ultrahigh dose rate FLASH irradiation (radiation exposed in an instant, like flash) could specifically spare normal tissue from ionizing radiation (IR)-induced detrimental outcomes while obtaining an equivalent tumor response to conventional dose rate (CONV) irradiation (the so-called "FLASH effect") in controlling lung tumors in the animal models, indicating a promising potentiality of FLASH RT in future clinical applications. FLASH radiation is recognized as an IR modality that delivers doses at dose rates far exceeding those currently used in clinical practice (17). In the aforementioned study, C57BL/6J mice were subjected to single bilateral thoracic irradiation with a dose of up to 17 Gy. IR-induced acute pneumonitis and late pulmonary fibrosis were both significantly repressed by 4.5-MeV electrons at an ultrahigh dose rate (≥60 Gy/s) in comparison with CONV irradiation (4.5-MeV electrons or γ-rays, 0.03 Gy/s). Mechanistically, based on single-cell RNAseq analysis, Favaudon and coworkers (18) identified that FLASH irradiation was less efficient than CONV radiation in up-regulating the expression of *Tgfb1* (the gene that encodes inflammatory factor TGF-β) at 4 d post-IR in mouse lung tissues. Given that TGF-β plays a pivotal role in the inflammatory process such as pulmonary fibrosis, the characteristic of FLASH in protecting normal tissues from radiation-induced detrimental outcomes might closely be correlated with IR-induced inflammation (18). Nonetheless, whether normal tissue toxicities could be reduced by FLASH radiation upon radioimmunotherapy remains elusive. Meanwhile, upon checkpoint blockade, the differential inflammatory process within CONV and FLASH IR-irradiated tissues merits further investigation.

Radiation injury-induced inflammation could be initiated by the proinflammatory death of damaged cells, among which pyroptosis is quite pivotal (19). The basic mechanism of pyroptosis is attributed to the cleavage of a family of proteins called gasdermin at the intermediate junction to release autoinhibition of the gasdermin-N domain, allowing it to insert into cell membranes to form large oligomeric pores and cause lytic immunogenic cell death (ICD) that elicits immune cell recruitment (20). Although it has long been believed that pyroptosis is inflammatory caspase (such as Caspase-1,-4,-5,-11)–mediated cell death caused by the cleavage of gasdermin D (21), other members within the gasdermin family have recently been reported to be cleaved by noninflammatory caspases (22), even granzymes (23). For instance, gasdermin E (GSDME) is demonstrated to be cleaved at its middle linker by granzyme B (GzmB), which generates the N-terminal domain of GSDME (GSDME-NT) and performs its pore-forming activity on the cell membrane (24). Nevertheless, the roles of pyroptosis within tissues exposed to radiation with differential dose rates remain to be elucidated.

In this study, the different intestinal deleterious outcomes along with distinct inflammatory mechanisms between CONV and FLASH X-ray irradiation in the case of PD-L1 blocking were investigated. Our study demonstrated that CONV whole abdominal irradiation (WAI) was much more efficient in evoking $CD8^+$ cytotoxic T lymphocyte (CTL) recruitment in the intestinal crypts than FLASH X-ray irradiation when PD-L1 was abrogated, leading to more severe GSDME-mediated pyroptotic crypt cell death that in turn induced more excessive CTL infiltration. The mechanism was attributed to the differences in eliciting the cytosolic double-stranded DNA (dsDNA) between FLASH and CONV irradiation, which made FLASH X-ray less efficient in activating the cGAS stimulator of interferon genes (STING) pathway. Contrarily, FLASH X-ray was as competent as CONV radiation to activate STING signals in irradiated mouse colon cancer cells, leading to equivalent antitumor immune response upon the abscopal tumor metastasis within anti–PD-L1–treated mice. Overall, the present study underpinned a promising role for FLASH X-ray RT combined with anticancer immunotherapy and demonstrated the mechanisms of the FLASH effect from an immunological perspective.

Results

Parameters and Dosimetry of the FLASH X-Ray Irradiation. As most RT practices are delivered using Mega-Volte (MV) X-rays produced by Linacs, an ideal candidate for the preclinical study would be a precisely tunable MV X-ray FLASH irradiation source. But until recently, most studies into FLASH radiation with low linear energy transfer have used electron beams (18, 25–27), presenting a limitation of clinical translation as the low tissue penetration. As a result, 6-MV high-energy X-ray with ultrahigh dose rate that was more attractive in clinical application than FLASH electrons was undertaken in the present study. The pulse structure of the FLASH X-ray is shown in *SI Appendix*, Fig. S1*A*, which revealed a full width at half maximum (FWHM) of the continuous electron micropulse of ∼5 ps. Nevertheless, the FWHM of the X-ray micropulse was around 10 ps due to broadening in the targeting procedure, resulting in an instantaneous dose rate of $\sim 1.85 \times 10^5$ Gy/s of the FLASH X-ray irradiation applied in this study. A 50-mm–thick lead secondary collimator was mounted close upstream of the sample (*SI Appendix*, Fig. S1*B*), while a diamond detector was installed at the entrance of the collimator to monitor the X-ray (*SI Appendix*, Fig. S1*C*). A monitor film was placed on the abdominal surface of the irradiated mouse (*SI Appendix*, Fig. S1 *D* and *E*). During FLASH irradiation, the delivered mean dose rate (110 to 120 Gy/s) depended on the beam current and source–surface distance (SSD) (*SI Appendix*, Fig. S1*F*), while the total given dose was set by regulating the width of the macropulse (*SI Appendix*, Fig. S1*A*) at different dose rates. The corresponding FLASH (*SI Appendix*, Fig. S1*G*) or CONV (*SI Appendix*, Fig. S1*H*) dose distribution of an EBT3 film mounted at 8-mm depth in solid water that simulated the center depth of the mouse abdomen illustrated the horizontal (*SI Appendix*, Fig. S1*I*) and vertical (*SI Appendix*, Fig. S1*J*) dose profiles of WAI, indicating that the central dose of FLASH IR was 15% higher than the mean dose (the blue curve). The electron beam was monitored in real time by a fast current transformer installed upstream of the target (*SI Appendix*, Fig. S1*F*), and a typical beam current curve in a 115-ms macropulse is shown in *SI Appendix*, Fig. S1*K*, which is consistent with the amplitude curve of the diamond detector (*SI Appendix*, Fig. S1*L*) in trend and length. The good linearity between dose

(given by ionization chamber) and monitor units (given by diamond monitor) (*SI Appendix*, Fig. S1*M*), as well as the relationship between dose rates measured by the ionization chamber and diamond monitor (*SI Appendix*, Fig. S1*N*), confirmed the reliability of the dosimetry system, ensuring the accurate dose delivery of FLASH X-ray irradiation in this study.

FLASH X-Ray Minimizes Mouse Enteritis in the Context of PD-L1 Blockade. PD-L1, also known as CD274 or B7 homolog 1 (B7-H1), is a critical immune checkpoint that mainly suppresses adaptive immune response through the interaction with its receptor PD-1 on the membrane of $CD8^+$ T cells (28), which maintains systemic immune tolerance in vivo. Therefore, blocking the function of either PD-L1 or PD-1 could significantly activate the antitumor immune response while aggravating the immune-related adverse events in normal tissues (29), among which dermatological toxicity and gastrointestinal disorders occur most frequently (30). Coincidentally, radiation-induced gastrointestinal toxicity is also a prevailing concern in patients receiving abdominopelvic radiation therapy, with more than 60% of patients experiencing symptoms of abdominal pain, diarrhea, or even intestinal obstruction during RT (31). As a result, mice were irradiated in the whole abdomen in the present study to demonstrate the acute and chronic intestinal radiation damage upon PD-1/PD-L1 blockade.

It is worth noting that PD-L1 was mainly expressed in mouse intestinal crypts (*SI Appendix*, Fig. S2 *A–C*) and was evoked by 13-Gy CONV (~0.03 Gy/s) WAI at 2 to 5 d post-IR (*SI Appendix*, Fig. S2*D*), indicating a potential function in negative immune regulation within the intestinal crypts. To abrogate the PD-1/PD-L1 signaling, PD-L1 knockout (KO) mice were studied and the lack of PD-L1 expression was determined by Western blotting analysis of various tissues derived from PD-L1 KO mice and their wild-type (WT) C57BL/6 cohorts (Fig. 1*A*). Fluorescein isothiocyanate (FITC)–dextran assay indicated that after 13-Gy abdominal CONV X-ray irradiation, the FITC levels in the peripheral blood of PD-L1 KO mice were notably higher than those in the WT counterparts (Fig. 1*B*), suggesting a much more increased gut permeability induced by PD-L1 checkpoint blockade during CONV irradiation. Surprisingly, FLASH WAI at the same dose notably ameliorated the integrity of mouse intestinal epithelium. As shown in Fig. 1 *C* and *D*, histopathological analysis of the proximal small intestines confirmed that classical pathogenic patterns such as severe crypt loss and grievous epithelial atrophy in PD-L1 KO mice exposed to CONV WAI were dramatically

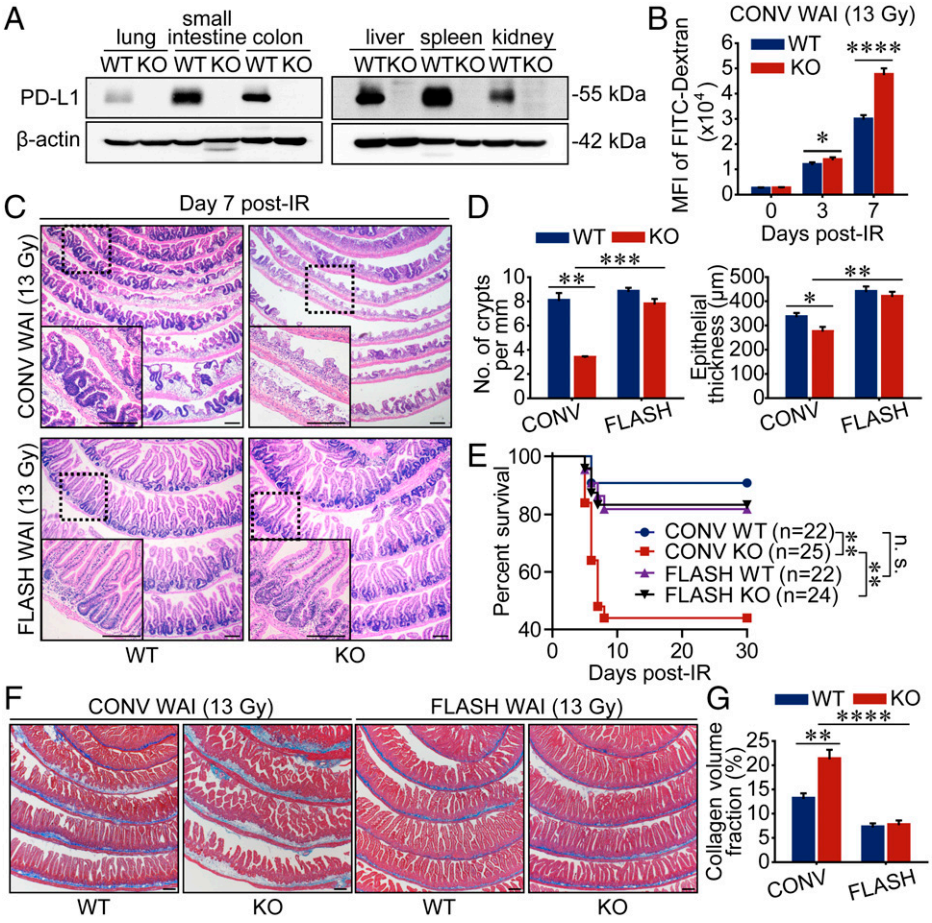

Fig. 1. FLASH X-ray minimizes mouse enteritis in the context of PD-L1 blockade. (*A*) Western blot analysis of PD-L1 expression levels in various organs from WT and PD-L1–deficient mice. (*B*) The gut permeability of mice undergoing 13-Gy CONV WAI was determined by detecting the intensity of fluorescence of FITC-dextran ($n = 6$ mice per group). MFI, mean fluorescence intensity. (*C* and *D*) Representative pictures of hematoxylin and eosin (H&E)-stained sections of proximal intestines sampled at 7 d after 13-Gy WAI are shown (*C*), and the numbers of crypts per millimeter and epithelial thickness were quantified (*D*) ($n = 3$ mice per group). (*E*) WT and PD-L1 KO mice were exposed to 13-Gy CONV or FLASH WAI. Kaplan–Meier survival analysis of mice was performed. (*F* and *G*) Representative pictures of Masson-stained sections of proximal intestines sampled at 6 mo after 13-Gy WAI are shown (*F*), and intestinal fibrosis was quantified by Image J (*G*) ($n = 6$ mice per group). Data represent three (*A–D*) or two (*E–G*) independent experiments. Error bars indicate SEM. $^*P < 0.05$, $^{**}P < 0.01$, $^{***}P < 0.001$, $^{****}P < 0.0001$, and no significance (n.s.) were determined by a two-sided Student's *t* test (*B*, *D*, and *G*) or determined by a log-rank test (*E*). (Scale bars, 200 μm.)

relieved in mice irradiated by 13-Gy FLASH X-ray. Furthermore, although 13-Gy FLASH X-ray caused a comparable survival fraction with CONV WAI in WT mice, which was similar to that in a recent study based on proton FLASH abdominal irradiation (32), FLASH WAI notably ameliorated mouse survival (83.3%) in PD-L1 KO mice when compared with CONV irradiation (44%) (Fig. 1*E*). Interestingly, obvious hair depigmentation delimited to the radiation field was observed in all surviving mice at 6 mo post-IR regardless of dose rates (*SI Appendix*, Fig. S2*E*).

Using the same FLASH X-ray device undertaken in the present study, Zhu et al. (33) revealed significantly diminished proinflammatory cytokines (e.g., TNF-α and IL-6) in the peripheral blood of mice being irradiated by FLASH abdominal radiation at the late stage of IR exposure. To further investigate the long-term consequences of FLASH WAI, Masson staining analysis was performed to detect the intestinal fibrosis of irradiated mice. As shown in Fig. 1 *F* and *G*, surviving PD-L1 KO mice exhibited higher levels of chronic intestinal fibrosis than WT animals 6 mo after 13-Gy CONV WAI. As expected, FLASH WAI considerably reduced the chronic intestinal inflammation in PD-L1 KO mice (Fig. 1 *F* and *G*). Together, these findings suggested that FLASH X-ray drastically spared PD-L1–deficient mice from 13-Gy WAI-evoked severe acute enteritis and chronic intestinal fibrosis.

FLASH X-Ray Impedes the Cascade Feedback of CTL-Induced Pyroptosis. A recent study based on single-cell RNAseq analysis of isolated mouse crypt cells revealed increased crypt-associated immune cells after CONV WAI (34). By reanalyzing the data of the aforementioned study, it was demonstrated that $CD8^+$ T lymphocytes were remarkably increased in number (*SI Appendix*, Fig. S3*A*) and proportion (*SI Appendix*, Fig. S3*B*) after 12-Gy WAI. To confirm the T cell infiltration in the intestinal crypts induced by IR exposure, the percentage of $CD8^+$ T lymphocytes in the mouse crypts was examined by flow cytometer. As shown in *SI Appendix*, Fig. S3 *C* and *D*, the proportion of $CD8^+$ T lymphocytes was ∼5% in the intestinal crypts of both PD-L1 WT and KO mice during the physiological state. Under CONV X-ray irradiation, the CTL percentage of intestinal crypts in PD-L1–deficient mice was further increased than in their WT cohorts (from ∼12 to 22.7%) (Fig. 2 *A* and *B*). Interestingly, FLASH irradiation notably attenuated the CTL ratio by nearly half in the PD-L1 KO crypts to 11.9% in comparison with CONV WAI (Fig. 2 *A* and *B*). To evaluate whether this reduction of CTL percentage after FLASH WAI was attributed to the maintaining of crypt architecture and epithelial cell number by attenuating the direct radiation damage or was attributed to the decrease of T cell recruitment, an in vitro study based on three-dimensional cultured organoids of intestinal crypts was performed to examine the differences of direct intestinal damage upon FLASH and CONV X-ray irradiation. And the dose distribution was shown in the form of profiles (*SI Appendix*, Fig. S3 *E* and *F*). As shown in Fig. 2 *C* and *D*, the survival rates of crypt organoids subjected to equal doses of CONV or FLASH irradiation were almost the same, suggesting a much more excessive infiltration of CTLs into crypts under CONV WAI than FLASH X-ray irradiation in PD-L1 KO mice.

$CD8^+$ T lymphocytes exert the cell-killing function primarily by secreting perforin and serine proteases such as GzmB. Recent data have indicated that CTL-derived GzmB plays a critical role in driving pyroptotic death in tumor cells by cleaving the newly discovered pyroptosis executive protein GSDME (22) to evoke membrane pore formation and membrane permeabilization (24). Therefore, the expression levels of cleaved GSDME were examined to ascertain the pyroptosis in the intestinal crypts of mice being irradiated by different dose rates. Indeed, IR-induced GSDME cleavage was further enhanced by PD-L1 abrogation at 72 to 120 h after CONV WAI, which was accompanied by a robust GzmB expression and Caspase-3 activation in the intestinal crypts (Fig. 2 *E* and *F*), since GzmB could also cleave Caspase-3. Administration of FTY-720, a sphingosine-1-phosphate receptor agonist that blocked the egress of T cells from lymphoid tissues (35, 36), dramatically abrogated CTL infiltration (*SI Appendix*, Fig. S3 *G* and *H*) and GSDME cleavage (Fig. 2 *G* and *H*) within intestinal crypts 72 h after CONV WAI, indicating that GSDME-mediated pyroptotic cell death was mainly regulated by excessively infiltrated CTLs. Of note, the expression levels of GSDME-NT in the PD-L1 KO crypts were drastically decreased by FLASH X-ray irradiation (Fig. 2 *I* and *J*), indicating a reduced intestinal pyroptosis in FLASH-treated animals. Proinflammatory cell death such as pyroptosis always elicits further immune cell recruitment by releasing damage signals, so-called damage-associated molecular patterns (DAMPs), into the extracellular milieu (37). To clarify whether GSDME-induced pyroptosis could, in turn, recruit more CTLs and thus evoke excessive T cell accumulation within intestinal crypts, GSDME was knocked down by short hairpin RNA (shRNA) coated by adeno-associated virus (AAV) (Fig. 2 *K*–*N*), and the T cell proportion was examined. Notably, GSDME knockdown considerably restrained the exceeding CTL accumulation within PD-L1 KO crypts at 3 d after CONV WAI (Fig. 2 *O* and *P*), indicating a necessity of GSDME-mediated pyroptosis for excessive CTL recruitment. The histopathological analysis further confirmed a reverse of radiation enteritis in GSDME-abrogated mice being irradiated by CONV WAI (Fig. 2 *Q* and *R*). Altogether, our data suggested that FLASH X-ray protected PD-L1 KO mice from GSDME-mediated pyroptosis, in comparison with CONV irradiation, which further alleviated the detrimental CTL infiltration and thus impeded the inflammatory feedback driven by ICD.

FLASH X-Ray Elicits Less cGAS-STING Activation in the Intestinal Crypts. To further explore the differential molecular drivers of T cell infiltration initiated by radiation modalities with different dose rates, we next sought to investigate the signaling pathways involved in the recruitment of $CD8^+$ T cells. The migratory behavior and recruitment of leukocytes are mainly governed by chemotactic cytokines. In 2019, the cooperation between CCL5 and CXCL9 was reported to be critical for T cell engraftment and immune attack in various tumors such as breast, colon, and lung cancers and gynecological solid tumors (38). Several recent studies also investigated whether chemokines of CCL5, CXCL9, CXCL10, and CXCL11 were strongly associated with $CD8^+$ T cell infiltration in pancreatic ductal adenocarcinoma, as well as head and neck squamous cell carcinoma (39, 40). However, whether these chemokines orchestrated the infiltration of T cells in the irradiated crypts was not well understood. In this study, the messenger RNA (mRNA) expression levels of *Ccl5*, *Cxcl9*, *Cxcl10*, and *Cxcl11* in mouse intestinal crypts irradiated by CONV and FLASH irradiation were examined by quantitative real-time PCR (qRT-PCR). As shown in Fig. 3*A*, chemokines in the intestinal crypts had been significantly up-regulated by CONV WAI since 24 h post-IR and were further increased the next day. Importantly, FLASH WAI considerably attenuated the expression levels of

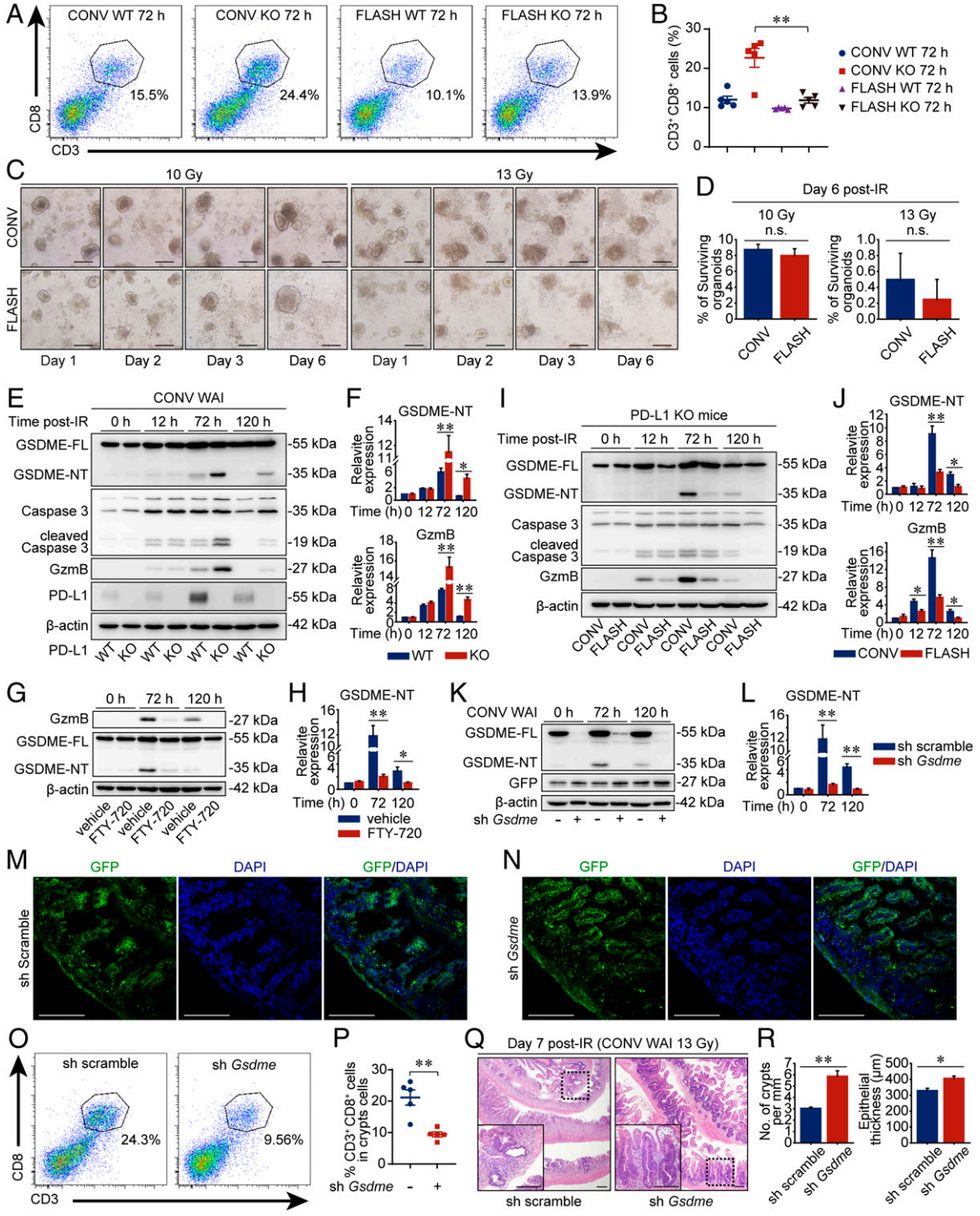

Fig. 2. FLASH X-ray impedes the cascade feedback of CTL-induced pyroptosis. (*A* and *B*) Flow cytometric analysis of $CD3^+CD8^+$ cells in the intestinal crypts at 3 d after 13-Gy CONV or FLASH WAI. Data are presented as representative plots (*A*) and quantified percentages (*B*) ($n = 5$ mice per group). (*C* and *D*) Organoids derived from isolated intestinal crypts of PD-L1 KO mice were subjected to 10- or 13-Gy X-ray irradiation. Representative pictures of the same microscopic fields at the indicated time post-IR are displayed (*C*). The percentages of surviving organoids (intact/refractive) were calculated on day 6 after irradiation (*D*). (*E* and *F*) Western blot analysis of protein expression levels in the crypts of mice exposed to 13-Gy CONV WAI. Representative pictures are shown (*E*). The relative ratio of GSDME-NT and GzmB to β-actin was normalized to the "WT 0 h" group (*F*). GSDME-FL, full length of GSDME. (*G* and *H*) PD-L1–deficient mice received FTY-720 as described in Materials and Methods. The protein expression levels of GSDME in the crypts were determined by immunoblot analysis and representative immunoblot pictures are shown (*G*). The relative ratio of GSDME-NT to β-actin was normalized to the "vehicle 0 h" group (*H*). (*I* and *J*) Immunoblot analysis of protein levels in crypts of PD-L1 KO mice being irradiated. Representative pictures are shown (*I*). The relative ratio of GSDME-NT and GzmB to β-actin was normalized to the "CONV 0 h" group (*J*). (*K* and *L*) The expression levels of GSDME and GFP in the crypts of irradiated AAV-sh *Gsdme*-EGFP transfected mice were detected by immunoblot analysis, and representative immunoblot pictures are shown (*K*). The relative ratio of GSDME-NT to β-actin was normalized to AAV-sh scramble-EGFP transfected control group (*L*). (*M* and *N*) GFP expression in the small intestines of AAV-sh scramble-EGFP (*M*) or AAV-sh *Gsdme*-EGFP (*N*) transfected mice at day 3 post-IR are shown. (*O* and *P*) Crypt-infiltrated $CD3^+CD8^+$ cells of mice 3 d after WAI were tested by flow cytometric analysis (*O*), and data are presented as quantified percentages (*P*) ($n = 5$ mice per group). (*Q* and *R*) Representative pictures of H&E-stained sections of proximal intestines sampled at 7 d after CONV WAI are shown (*Q*), and the numbers of crypts per millimeter and epithelial thickness were quantified (*R*) ($n = 3$ mice per group). Data are pooled from two [(*A* and *B*), (*O* and *P*)] or three (*E*–*L*) independent experiments or represent three independent experiments [(*C* and *D*), (*M* and *N*), (*Q* and *R*)]. Error bars indicate SEM. $^*P < 0.05$, $^{**}P < 0.01$, and n.s. were determined by a two-sided Student's *t* test. (Scale bars, 200 μm.)

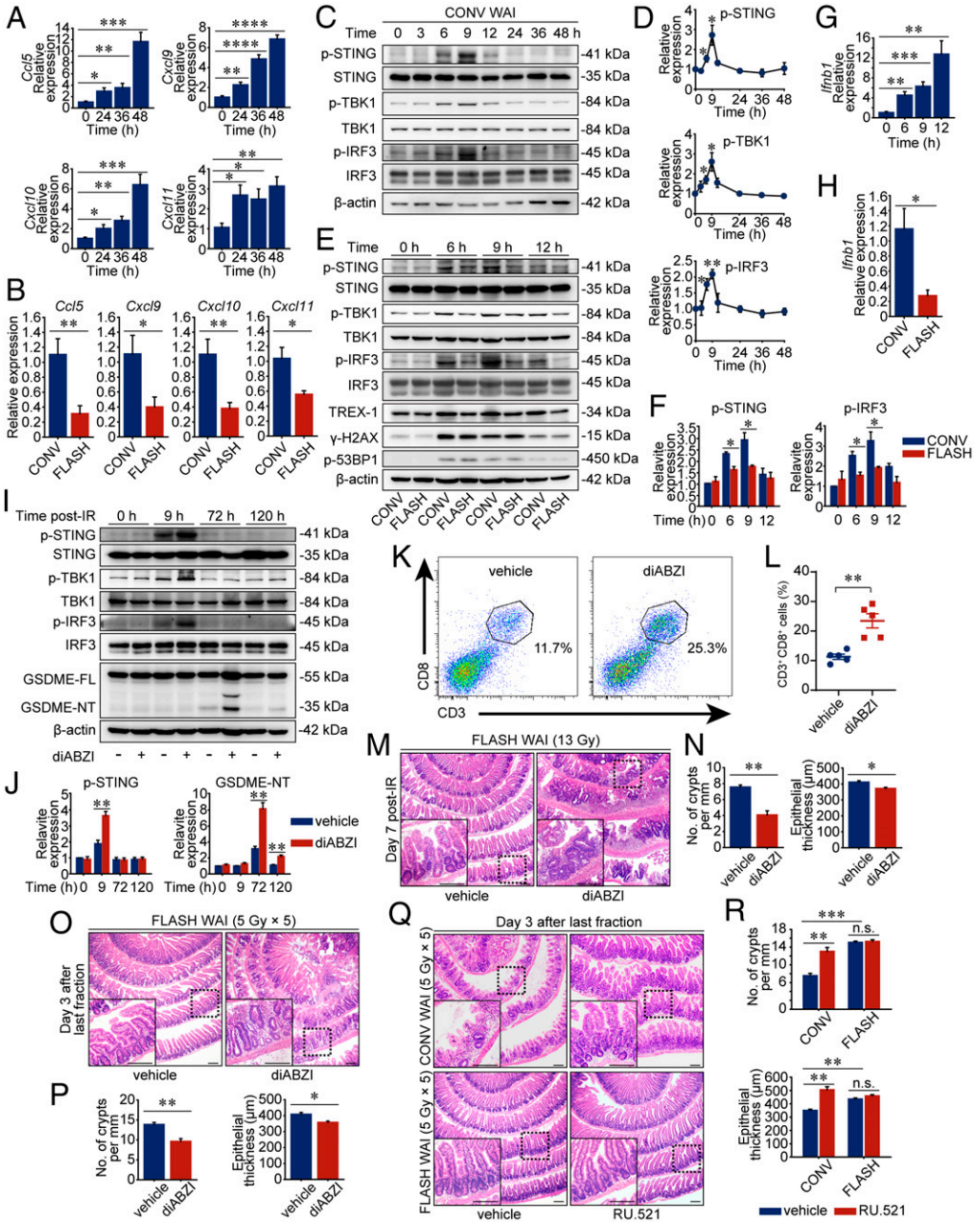

Fig. 3. FLASH X-ray elicits less cGAS-STING activation in the intestinal crypts. (*A*) PD-L1 KO mice were exposed to 13-Gy CONV WAI. The relative mRNA expression levels of *Ccl5*, *Cxcl9*, *Cxcl10*, and *Cxcl11* from the intestinal crypts were determined by qRT-PCR (n = 5 mice per group). (*B*) The relative mRNA expression levels from the intestinal crypts were determined by qRT-PCR at 48 h after 13-Gy CONV or FLASH irradiation (n = 5 mice per group). (*C* and *D*) Western blot analysis of protein expression levels in the intestinal crypts of PD-L1 KO mice at the indicated time after 13-Gy CONV WAI. Representative immunoblot pictures are shown (*C*). The relative ratio of phosphorylated STING, phosphorylated TBK1, and phosphorylated IRF3 to β-actin was determined from the immunoblot quantification and was normalized to the control group (*D*). (*E* and *F*) Immunoblot analysis of protein expression levels in the intestinal crypts of PD-L1 KO mice at the indicated time after 13-Gy CONV or FLASH WAI. Representative immunoblot pictures are shown (*E*). The relative ratio of phosphorylated STING and phosphorylated IRF3 to β-actin was determined from the immunoblot quantification and was normalized to the "CONV 0 h" group (*F*). (*G*) PD-L1 KO mice were exposed to 13-Gy CONV WAI. The relative mRNA expression levels of *Ifnb1* from the intestinal crypts were determined by qRT-PCR (n = 5 mice per group). (*H*) The relative mRNA expression levels from the intestinal crypts were determined at 12 h after 13-Gy CONV or FLASH irradiation (n = 5 mice per group). (*I*–*N*) PD-L1–deficient mice were exposed to 13-Gy FLASH WAI and were treated with solvent or STING agonist, diABZI, immediately after irradiation. Representative pictures of the immunoblot analysis of protein expression levels in the intestinal crypts at the indicated time post-IR are shown (*I*). The relative ratio of indicated protein to β-actin was determined from the immunoblot quantification and was normalized to the "vehicle 0 h" group (*J*). Crypt-infiltrated $CD3^+CD8^+$ cells of mice at 3 d after WAI were determined by flow cytometric analysis (*K*), and data are presented as quantified percentages (*L*) (n = 5 mice per group). Representative pictures of H&E-stained sections of proximal intestines sampled at 7 d after FLASH WAI are shown (*M*), and the numbers of crypts per millimeter and epithelial thickness were quantified (*N*) (n = 3 mice per group). (*O* and *P*) C57BL/6 mice were exposed to fractionated FLASH WAI and were dosed with the intraperitoneal injections of diABZI and anti-mouse PD-L1 antibody as described in Materials and Methods. Representative pictures of H&E-stained sections of proximal intestines sampled on day 3 after the last fraction are shown (*O*), and the numbers of crypts per millimeter and epithelial thickness were quantified (*P*) (n = 3 mice per group). (*Q* and *R*) C57BL/6 mice were exposed to fractionated CONV or FLASH WAI and were dosed with the intraperitoneal injections of RU.521 and anti-mouse PD-L1 antibody as described in Materials and Methods. Representative pictures of H&E-stained sections of proximal intestines sampled on day 3 after the last fraction are shown (*Q*), and the numbers of crypts per millimeter and epithelial thickness were quantified (*R*) (n = 3 mice per group). Data are pooled from three (*A*–*J*) or two (*K* and *L*) independent experiments or represent three independent experiments (*M*–*R*). Error bars indicate SEM. *P < 0.05, **P < 0.01, ***P < 0.001, ****P < 0.0001, and n.s. were determined by a two-sided Student's t test. (Scale bars, 200 μm.)

these chemokines to nearly half of those in CONV X-ray–irradiated crypts at 48 h post-IR (Fig. 3*B*), indicating a decreased chemotaxis signal of T lymphocytes within intestinal crypts upon this ultrahigh dose rate radiation modality.

It is well known that genes encoding the aforementioned chemokines are up-regulated by the type I IFN-mediated signaling pathway stimulated by the cGAS-STING axis responding to cytoplasmic dsDNA fragments (5, 11, 40). IR-induced chromosomal fragments are recognized by the cytosolic nucleic acid sensor cGAS, facilitating cGAMP synthesis from ATP and GTP. cGAMP then activates STING that phosphorylates TANK-binding kinase 1 (TBK1) and IFN regulatory factor 3 (IRF3) to trigger expression and secretion of type I IFNs, including IFN-β (41). As a result, the activity of the cGAS-STING signaling pathway within mouse crypts was determined by Western blot assay, which revealed notably increased STING, TBK1, and IRF3 phosphorylations at 6 to 9 h after CONV WAI (Fig. 3 *C* and *D*). Of note, FLASH X-ray irradiation dramatically diminished the activity of the cGAS-STING signaling pathway (Fig. 3 *E* and *F*) and reduced STING-mediated *Ifnb1* (the gene that encoded IFN-β) expression that was provoked by CONV WAI 12 h post-IR (Fig. 3 *G* and *H*). To further demonstrate the role the STING-IFN signaling pathway played during intestinal pyroptosis induced by WAI with differential dose rates, linked dimeric amidobenzimidazole (diABZI), an enhanced STING agonist (42), was injected intraperitoneally directly after 13-Gy FLASH WAI to activate STING signal artificially (Fig. 3 *I* and *J*). Intriguingly, diABZI administration considerably enhanced the CTL proportion within FLASH-irradiated PD-L1–deficient mouse crypts to ∼23.4% (Fig. 3 *K* and *L*), which was almost comparable to that in CONV X-ray–irradiated counterparts. Moreover, FLASH IR-induced pyroptotic cell death (Fig. 3 *I* and *J*) along with enteritis (Fig. 3 *M* and *N*) in PD-L1 KO mice was also exacerbated by STING stimulation.

Furthermore, immunocompetent WT mice being irradiated by fractionated FLASH irradiation (5 Gy at a time for 5 consecutive days, 25 Gy in total, i.e., 5 Gy × 5) combined with anti–PD-L1 antibody administration, a more clinically relevant scenario in radioimmunotherapy, also revealed a similar aggravation of enteritis induced by diABZI treatment (Fig. 3 *O* and *P*). Contrarily, RU.521 that impeded cGAS activity notably ameliorated the intestinal architecture of mice being treated with fractionated CONV WAI combined with an anti–PD-L1 antibody (Fig. 3 *Q* and *R*). Intriguingly, RU.521 failed to further improve the integrity of the intestinal epithelium of FLASH X-ray–irradiated mice undergoing checkpoint blockade (Fig. 3 *Q* and *R*). These findings further confirmed that the relatively inadequate cGAS-STING activity within intestinal crypts exposed to FLASH radiation contributed to sparing mice from intestinal pyroptosis and enteritis upon radioimmunotherapy.

FLASH X-Ray Produces Less Cytosolic DNA in the Intestinal Crypts. The activity of the cGAS-STING signal was regulated mainly by the content of cytosolic dsDNA. To further elucidate the mechanism of FLASH IR in regulating the cGAS-STING activity, the levels of cytosolic dsDNA were examined using PicoGreen, a dsDNA-specific vital dye. As shown in Fig. 4*A*, significantly lower levels of dsDNA were present in the cytoplasmic fraction of intestinal organoids exposed to 8-Gy FLASH X-ray than CONV X-ray at the same dose. Given the cytoplasmic dsDNA fragments were reported to be eliminated by 3′ repair exonuclease-1 (TREX-1) (43), the expression levels of TREX-1 within intestinal organoids exposed to WAI were detected in vitro. It was worth noting that the TREX-1 expression levels in FLASH X-ray–irradiated organoids of intestinal crypts were no higher (even lower) than those in CONV IR-irradiated ones (Fig. 4 *B* and *C*), indicating that relatively more activated STING signal that presented upon CONV irradiation than FLASH X-ray (Fig. 4 *B* and *C*) was due to more grievous primary DNA damage rather than TREX-1 elimination. Surprisingly, the Western blot assay revealed that the expression levels of both γ-H2AX and phosphorylated 53BP1 were almost the same in the intestinal crypt organoids irradiated by FLASH and CONV X-rays (Fig. 4 *B* and *C*), indicating that FLASH X-ray evoked as much damage in the genomic DNA as CONV irradiation did. Immunofluorescent assay further verified that 4-Gy FLASH X-ray elicited equivalent 53BP1 foci in the human intestinal epithelial HIEC-6 cells with CONV X-ray (Fig. 4 *D* and *E*). Notably, 53BP1 was found to elicit a differential response between FLASH and CONV electrons in MRC5 and IMR90 human lung fibroblast cells by Favaudon and coworkers (18), which was different from our results. In addition to the cell-specific mechanisms of the recruitment of 53BP1 to the DSB foci, the main reason might be that the dose rate of FLASH X-ray applied in our study was much lower than that of FLASH electron beams undertaken by Favaudon and coworkers (18). Specifically, given the single-macropulse mode applied in our study, an actual dose rate in the pulse was only 110 to 120 Gy/s, which was equal to the mean dose rate itself. However, the dose rate in the pulse used in Favaudon and coworkers' (18) study was more than 1×10^7 Gy/s (18), a dose rate much more likely to spare normal cells from genomic DNA damage by inducing oxygen depletion (25). Similarly, Levy et al. (44) also demonstrated that 14-Gy abdominal FLASH irradiation with a dose rate in the pulse of 4.0×10^5 Gy/s could induce less genomic DNA damage in the intestinal crypt stem cells than CONV electron beams did, taking γ-H2AX foci as endpoints.

On the other hand, the capability of FLASH in sparing mouse intestine from pyroptosis by minimizing IR-induced cGAS-STING activity raised the concern that this might translate to a loss of antitumor efficacy. Therefore, we sought to investigate the phosphorylations of STING, TBK1, and IRF3 within colorectal tumor cells after being irradiated by different radiation modalities. Intriguingly, when compared with CONV X-ray at the same doses, FLASH IR equally enhanced expression levels of phosphorylated proteins within the STING pathway (*SI Appendix*, Fig. S4 *A* and *B*). Meanwhile, 8-Gy FLASH X-ray induced roughly equal amounts of cytoplasmic dsDNA fragments to CONV IR in MC38 tumor cells (*SI Appendix*, Fig. S4*C*). Since PicoGreen also stained mitochondrial DNA, MitoTracker was applied simultaneously to indicate the mitochondria. As shown in Fig. 4*F*, most of the PicoGreen-stained areas in the cytoplasm of MC38 cells were not overlapped with the areas traced by MitoTracker, indicating the accumulation of cytosolic dsDNA induced by CONV or FLASH X-ray IR (Fig. 4*G*). Altogether, the differences of FLASH X-ray in activating the cGAS-STING signal between tumor cells and normal cells suggested a different mechanism involved in the interaction between FLASH IR and DNA molecules.

Fractionated FLASH X-Ray Was As Competent As CONV IR in Eradicating Abscopal Tumors. Recently, Eggold et al. (45) indicated that abdominopelvic FLASH irradiation could maintain the ability to increase intratumoral $CD8^+$ T cell infiltration and enhance the efficacy of anti–PD-1 therapy in ovarian cancers. To investigate whether FLASH radiation was as efficient as CONV radiation in eliciting the abscopal antitumor immune response, MC38 tumor cells were implanted on the

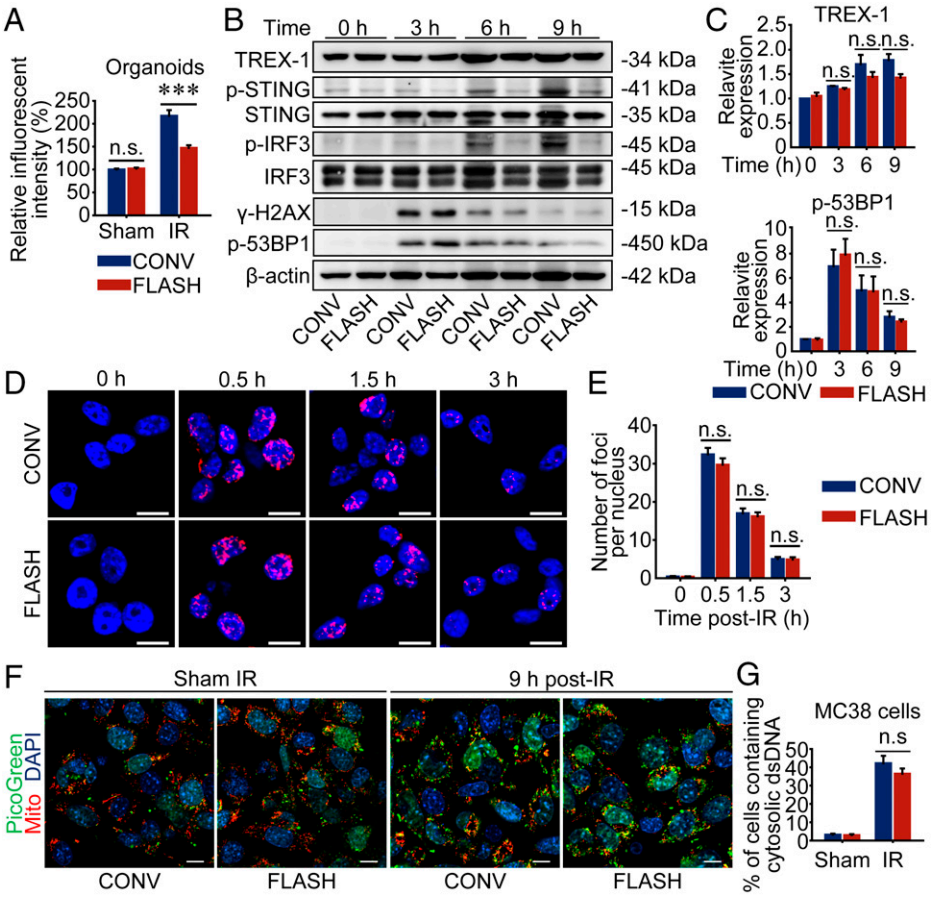

Fig. 4. FLASH X-ray produces less cytosolic dsDNA in the intestinal crypts. (*A*) Organoids derived from isolated intestinal crypts of PD-L1 KO mice were subjected to 8-Gy X-ray of CONV or FLASH irradiation, and the cytoplasm was extracted 9 h post-IR to quantify the cytosolic dsDNA by detecting the fluorescence intensity of PicoGreen-stained dsDNA. (*B* and *C*) Organoids derived from isolated intestinal crypts of PD-L1 KO mice were subjected to 8-Gy CONV or FLASH irradiation. The protein of organoids was extracted for Western blot analysis. Representative pictures are displayed (*B*). The relative ratio of indicated protein to β-actin was determined from the immunoblot quantification and was normalized to the "CONV 0 h" group (*C*). (*D*) Representative images of 53BP1 fluorescent staining in nuclei of HIEC-6 cells exposed to 4-Gy CONV or FLASH X-ray. (*E*) Quantification of nuclear 53BP1 foci. (*F* and *G*) MC38 cells were exposed to 8-Gy CONV or FLASH irradiation and incubated with PicoGreen (green) and MitoTracker (red) 9 h post-IR for 1 h to stain cytosolic dsDNA and mitochondria, respectively. Confocal images are shown (*F*) and cytosolic dsDNA accumulations were quantified (*G*). Data representthree independent experiments [(*A*), (*D* and *E*), (*F* and *G*)] or are pooled from three independent experiments (*B* and *C*). Error bars indicate SEM. ***$P < 0.001$ and n.s. were determined by a two-sided Student's *t* test. (Scale bars, 10 μm.)

left (primary, irradiated) and right (secondary, nonirradiated) flanks of immunocompetent C57BL/6 mice (Fig. 5*A*). Ten days after primary tumor implantation, mice were randomized to each group based on tumor volumes and were irradiated by X-ray delivered with hypofractionated regimens (5 Gy × 5), either by FLASH X-ray (*SI Appendix*, Fig. S5*A*) or by CONV X-ray (*SI Appendix*, Fig. S5*B*). The anti–PD-L1 antibody was administered as indicated in Fig. 5*A*. The two-dimensional profile of radiation fields revealed a relatively even dose distribution within irradiated tumor sites of both CONV and FLASH IR, as well as virtually absent dose delivery at abscopal tumor sites (*SI Appendix*, Fig. S5 *C–H*). To investigate whether FLASH RT could augment antitumor immunity equivalent to CONV IR, intratumoral $CD8^+$ T cells were evaluated. As shown in *SI Appendix*, Fig. S6 and Fig. 5*B*, anti–PD-L1 as a monotherapy hardly elicited T cell infiltration within both primary tumors and secondary tumors, which obtained an extremely slight effect on restraining MC38 tumor growth (Fig. 5 *C* and *D*), resulting in 100% of mice eventually succumbing to either excessive tumor volumes or diameters (Fig. 5*E*). Notably, both CONV and FLASH RT provoked robust CTL infiltration within anti–PD-L1–treated primary tumors (*SI Appendix*, Fig. S6*A* and Fig. 5*B*) accompanied by almost equivalent eradication of primary tumors 3 wk after treatment (Fig. 5*C*). Although FLASH RT failed to elicit adequate antitumor immunity in all tumor metastases, it still induced the intratumoral T cell response comparably to CONV radiation (*SI Appendix*, Fig. S6*B* and Fig. 5*B*), along with an equal elimination rate of metastatic burdens (Fig. 5*D*). Moreover, 57.1% of mice treated with the combination regimen were cured and achieved long-term survival regardless of FLASH RT or CONV RT (Fig. 5*E*), indicating an equal abscopal response and systemic antitumor immunity induced by FLASH and CONV X-ray when integrated with checkpoint blockade.

Discussion

Unlike irradiation modalities that alleviate collateral damage to radiosensitive organs by spatially increasing the dose delivery at tumor sites (such as intensity-modulated RT, stereotactic body RT, and image-guided RT), FLASH irradiation with an ultra-high dose rate has been demonstrated in multiple preclinical studies to widen the therapeutic window in the dimension of "dose rate" by sparing normal tissues from IR-induced deleterious outcomes while preserving an equivalent tumor response in comparison with CONV radiation treatment (16, 25, 46).

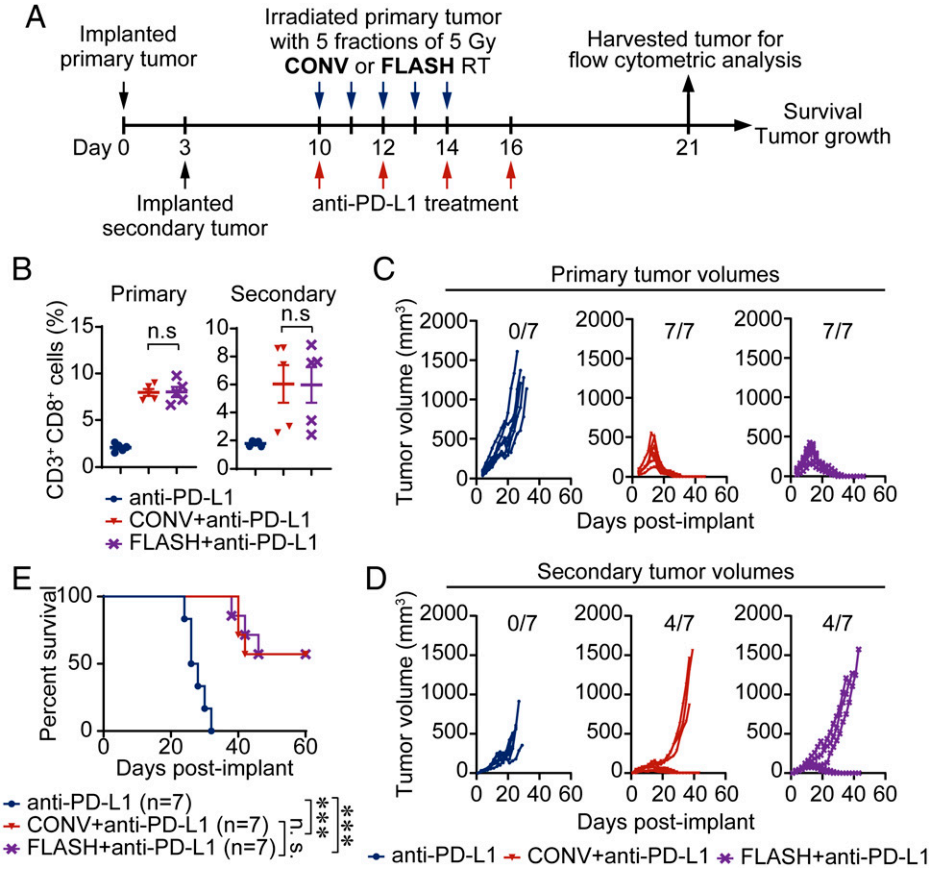

Fig. 5. Fractionated FLASH X-ray is as competent as CONV IR in eradicating abscopal tumors. (*A*) Schema for tumor radioimmunotherapy. (*B*) $CD3^+CD8^+$ cells within primary and secondary tumors 5 d after the last injection of anti–PD-L1 antibody were tested by flow cytometric analysis ($n = 5$ mice per group). The quantified percentages of $CD3^+CD8^+$ cells in tumors are presented. (*C* and *D*) Tumor growth curves of primary (*C*) and secondary (*D*) tumors subjected to the indicated treatments are shown, and the numbers of tumor-free mice are indicated. (*E*) Kaplan–Meier survival analysis of tumor-bearing mice undergoing the indicated treatments was performed. Data are pooled from two independent experiments (*B*) or represent two independent experiments (*C*–*E*). Error bars indicate SEM. ***$P < 0.001$ and n.s. were determined by a two-sided Student's *t* test (*B*) or determined by a log-rank test (*E*).

Therefore, we speculate that this ultrahigh dose rate radiation delivery mode is an ideal modality to specifically enhance tumor immunogenicity while overcoming the adverse responses during radioimmunotherapy.

It is worth noting that dosimetry at extremely high dose rates is one of the tough technological challenges in beam deliveries of FLASH radiation. In the present study, the active dosimeter containing a pinpoint ionization chamber, as well as an electrometer working in the integration mode, was used, and the decrease of ion collection efficiency in the chamber due to ion recombination in FLASH irradiation was carefully checked by computing and experiments. The relationship between dose rates measured by the ionization chamber and the diamond monitor indicated excellent linearity in a dose rate range of 1 to 1,000 Gy/s (*SI Appendix*, Fig. S1*N*), suggesting that the loss of ion collection efficiency was negligible when the mean dose rates were less than 1,000 Gy/s under the pulse structure applied in this study (*SI Appendix*, Fig. S1*A*). Dose distribution (*SI Appendix*, Figs. S1 *G–J* and S5 *C*, *E*, and *G*) and calibration (*SI Appendix*, Fig. S1 *K–M*) also demonstrated the stability and reliability of the FLASH X-ray irradiation devices.

Although clinical data comparing the sequences in which different treatments should be administered are largely missing in the setting of radioimmunotherapy, it is generally believed that unlocking immune checkpoints concomitant to RT would evoke more severe cumulative toxic effects than sequential administrations (8). Therefore, PD-L1 KO mice that underwent CONV or FLASH X-ray irradiation were applied as animal models to simulate the concurrent administration of RT with checkpoint blockade. Despite PD-L1 playing a pivotal role in suppressing autoimmune diseases (47, 48), the basal levels of intestinal T cell proportion (*SI Appendix*, Fig. S3 *C* and *D*), along with the intestinal epithelial integrity (*SI Appendix*, Fig. S7*A*), crypt proliferation (*SI Appendix*, Fig. S7 *B* and *C*), and intestinal fibrosis (*SI Appendix*, Fig. S7 *D* and *E*) within PD-L1–deficient mice were the same as those in WT ones. When undergoing FLASH X-ray irradiation, organoids of intestinal crypts exhibited significantly reduced cytosolic dsDNA (Fig. 4*A*) and less active cGAS-STING signal (Fig. 4 *B* and *C*) compared with CONV X-ray–irradiated cohorts. The relatively inactive STING pathway led to a decline in IR-induced *Ifnb1* transcription (Fig. 3*H*) in vivo that further reduced T cell intestinal chemotaxis (Fig. 3*B*). In CONV WAI, excessive T cell response within irradiated intestinal crypts further initiated a GzmB-mediated GSDME cleavage, which generated much more GSDME-NT driving pyroptotic cell death than FLASH IR did (Fig. 2 *I* and *J*). As proinflammatory ICD, intestinal pyroptosis drove not only direct epithelial cell loss but also T cell recruitment to enhance local immune response, which in turn enhanced the activity of GSDME cleavage, establishing inflammatory feedback comprising T cell infiltration (Fig. 2 *A* and *B*) and lethal pyroptotic cell death (Fig. 2 *E–R*). Interestingly, FLASH X-ray was able to evoke equivalent cytoplasmic dsDNA fragments (*SI Appendix*, Fig. S4*C*) and phosphorylations of STING, TBK1, and IRF3 (*SI Appendix*, Fig. S4 *A* and *B*) within mouse colorectal tumor cells when compared with CONV IR, resulting in a comparable abscopal intratumoral T cell response

(*SI Appendix*, Fig. S6*B* and Fig. 5*B*), as well as equal efficacies in eradicating metastatic burdens (Fig. 5*D*), in anti–PD-L1–treated mice. These data suggested that FLASH X-ray RT could notably enhance intestinal tolerance in the context of PD-L1 blockade while maintaining the abscopal tumor suppression, which dramatically widened the therapeutic window with invaluable therapeutic potential for the development of radioimmunotherapy.

Of note, it has long been recognized that photons with lower energies generally have higher relative biological efficiency (RBE), especially at low doses. Specifically, the mean photon energy of the FLASH X-ray was 1.36 MeV (*SI Appendix*, Fig. S8) while that of orthovoltage (160 to 320 kV) CONV X-rays was only around 60 to 80 keV (*SI Appendix*, Fig. S8), which might cause more intestinal damage by CONV irradiation under the same doses, and thus reduced the authenticity of the FLASH sparing effect. Using cobalt-60 (mean photon energy 1.25 MeV) as the reference, the RBE of 6-MV X-rays was around 1.0 and the RBE of 200-kV X-rays given by Favaudon et al. (16) was around 1.3, whereas the RBE of 180-kV X-rays at 4 to 13 Gy was calculated to be around 1.1 using the dose-effect curves given by Mestres et al. (49). Given that the RBE was highly variable and depended on the cell types being irradiated, the biological effects being assayed, irradiated doses, and even the filters of X-ray generators, it was inappropriate to conduct studies directly based on a specific RBE calculated from others. Therefore, in vitro experiments were carried out to measure and compare the RBEs between 160-kV and 6-MV CONV X-rays in eliciting genomic DNA damage and generating cytosolic dsDNA within intestinal crypt cells, which were demonstrated to be the core mechanisms of IR-induced mouse enteritis in the context of PD-L1 blockade. As shown in *SI Appendix*, Fig. S9, there seemed to be no difference in inducing genomic DNA damage (*SI Appendix*, Fig. S9 *A* and *B*) and in generating cytoplasmic dsDNA fragments (*SI Appendix*, Fig. S9*C*) between 6-MV CONV X-ray and 160-kV X-ray in the dose range of 4 to 8 Gy. Furthermore, 6-MV CONV X-ray was also undertaken to examine the survival rates of PD-L1 KO crypt organoids in vitro, which achieved the same survival fraction as the organoids subjected to equal doses of 160-kV X-ray irradiation (*SI Appendix*, Fig. S9 *D* and *E*), suggesting the same RBE between 160-kV and 6-MV X-ray irradiations under the irradiation conditions applied in this study.

Actually, the percentage depth dose (PDD) of X-rays was also pivotal in the clinical RT that was directly related to the absorbed dose in vivo. Of note, as shown in *SI Appendix*, Fig. S10, orthovoltage (225 and 320 kV) X-rays revealed a much better PDD consistency with 6-MV FLASH X-ray, compared with the 6-MV CONV X-ray. The maximum discrepancy of the PDD in mice, appearing on the back surface of the mice, between orthovoltage (225 and 320 kV) and FLASH X-rays was around 4%, whereas that between 6-MV CONV and FLASH X-rays was up to 16%. Consequently, orthovoltage (225 and 320 kV) X-rays instead of 6-MV X-ray were undertaken as the CONV control for FLASH X-ray irradiation in the in vivo studies.

At present, the "oxygen depletion" hypothesis is one of the most widely considered hypotheses to clarify the FLASH sparing effect at the mechanistic level. Nevertheless, recent data have challenged this hypothesis since FLASH radiation could hardly induce sufficient hypoxia within healthy oxygenated normal tissues (50). Coincidently, in the present study, FLASH X-ray irradiation with a mean dose rate of 110 to 120 Gy/s (instantaneous dose rate $\sim 1.85 \times 10^5$ Gy/s) also failed to notably reduce the genomic DNA damage when compared with CONV IR, taking 53BP1 and γ-H2AX as endpoints (Figs. 3*E* and 4 *B*–*E*). Intriguingly, however, FLASH X-ray irradiation elicited notably less cytosolic dsDNA (Fig. 4*A*) and lower cGAS-STING activity (Fig. 4 *B* and *C*) in the intestinal organoids than CONV IR, as well as a comparable systemic antitumor response (*SI Appendix*, Fig. S6 and Fig. 5 *B*–*E*) evoked by equivalent cytosolic dsDNA signaling within irradiated tumor cells (*SI Appendix*, Fig. S4 *A*–*C* and Fig. 4 *F* and *G*) to CONV radiotherapy. These aforementioned findings were difficult to clarify by the oxygen depletion hypothesis.

Therefore, we proposed the "DNA integrity" hypothesis to elucidate the mechanism of the FLASH sparing effect, suggesting that "relatively intact DNA integrity" within intestinal cells during the "instantaneous" (~120 ms) IR exposure was critical for FLASH X-ray in sparing PD-L1–deficient mice from detrimental enteritis. Specifically, during CONV radiation, the deposition of the radiation dose took hundreds of seconds, which meant part of DNA molecules had already been subjected to radiation energy sufficient to elicit breakage before the completion of dose delivery, thus inducing partial DNA damage and undermining DNA integrity. When damaged DNA molecules were further irradiated, the disturbance in genome integrity resulted in the generation of "extra" DNA fragments, which activated the cytoplasmic cGAS-STING system. In contrast, the dose deposition of FLASH irradiation was completed in ~100 ms, which can be considered instantaneous in terms of the biological process of DNA damage. This meant that during the dose deposition of FLASH IR, there was almost no chance for the occurrence of DNA breaks and instability similar to those generated during CONV irradiation before the complete deposition of equivalent dose and, hence, no generation of extra DNA fragments. Therefore, the activity of the cGAS-STING signaling pathway was dramatically reduced (*SI Appendix*, Fig. S11). On the other aspect, genomic instability had been recognized as a hallmark of cancer for more than a decade (51, 52), which was a direct consequence of DNA damage response deficiency making tumor cells susceptible to various physicochemical DNA damage triggers. As a result, in tumor cells, numerous DNA fragments were provoked and released into the cytoplasm even during FLASH radiation due to the intrinsic genome instability, which subsequently activated the cGAS-STING system and initiated systemic antitumor responses.

An improved understanding of the mechanism of the FLASH sparing effects was crucial for the optimization of clinical applications and the development of suitable accelerators. Unlike the oxygen depletion hypothesis that emphasized the significance of instantaneous dose rate (25, 27), the DNA integrity hypothesis focused more on the duration of dose delivery. That is, based on our data, the mean dose rate might be somewhat more pivotal than the instantaneous dose rate in eliciting the FLASH effect. Although this study elucidated the molecular mechanism of the FLASH effect in terms of immunology and provided an initial framework for future clinical applications of FLASH X-ray RT in combination with anticancer immunotherapy, only intestinal crypts and colorectal tumors were applied in this study. In the future, more organs and tumors, along with additional molecular probes detecting the instantaneous DNA damage and DNA integrity, are desperately needed to demonstrate the DNA integrity hypothesis much more directly.

Materials and Methods

A detailed description of the materials and experimental procedures is available in *SI Appendix, Materials and Methods*.

Materials and Methods Summary.

CONV and FLASH irradiation. An X-RAD 320iX Biological Irradiator (Precision X-ray) was used for WAI. CONV RT was performed by the Pxi SmART RAD system (Precision X-ray). In vitro studies were performed via a biological research irradiator (Rad Source; RS-2000 Pro). Detailed characters of the X-ray generators for CONV irradiation are listed in *SI Appendix*, Table S1. The FLASH irradiation was carried out using the platform for advanced RT research (PARTER) at the Chengdu THz Free Electron Laser facility (CTFEL) in China.

Mice and cell line. C57BL/6 mice and the PD-L1 KO mice with the C57BL/6 background were subjected to IR exposure at 8 to 10 wk of age. The study was conducted in compliance with local animal welfare laws and policies. All procedures were approved by the ethics committee of Soochow University. MC38 cells and HIEC-6 cells were purchased from ATCC and cultured at 37 °C in an incubator containing 5% CO_2.

Intestinal crypt organoid studies. Small intestinal crypts were isolated and subsequently used for Western blot analysis or further culture. Isolated crypts were suspended with Matrigel (Corning, no. 356231) and incubated with advanced DMEM/F12 medium (Thermo Fisher Scientific, no. 12634-010) that was supplemented with EGF (Peprotech, no. 315-09-100), Noggin (Peprotech, no. 250-38-5), R-spondin (Peprotech, no. 315-32-5), N2 (Thermo Fisher Scientific, no. 17502048), B27 (Thermo Fisher Scientific, no. 17504044), and Y-27632 dihydrochloride monohydrate (Sigma, no. Y0503). After being cultured for 2 d in vitro, organoids were exposed to CONV or FLASH irradiation at different doses.

Antibodies. The following antibodies were used: anti–PD-L1 (Abcam, no. ab213480), anti–Caspase-3 (CST, no. 9662), anti-GSDME (Abcam, no. ab215191), anti-Granzyme B (Abcam, no. ab255598), anti-STING (CST, no. 50494), anti–phospho-STING (Ser365) (CST, no. 72971), anti–TBK-1 (CST, no. 3504), anti–phospho-TBK-1 (Ser172) (CST, no. 5483), anti–IRF-3 (CST, no. 4302), anti–phospho-IRF3 (Ser396) (CST, no. 4947S), anti–γ-H2AX (phospho Ser139) (Abcam, no. ab81299), anti-53BP1 (Abcam, no. ab175933), anti–phospho-53BP1 (Ser25) (Abcam, no. ab70323), anti–TREX-1 (Santa Cruz, no. sc-133112), anti-GFP (Beyotime Inc., no. AG279), and anti–β-actin (Abcam, no. ab8226). For flow cytometry analysis, anti–CD3-APC (Biolegend, no. 100236) and anti–CD8-PE (Biolegend, no. 100707) were used.

AAV transfection. GSDME knockdown (AAV-sh *Gsdme*-EGFP) and control (AAV-sh scramble-EGFP) recombinant adeno-associated virus vectors 9 were purchased (GENECHEM Biotech) and injected into PD-L1 KO mice through the tail vein (5×10^{11} physical particles per mouse).

Agonist and inhibitor administration. The following agonists and inhibitors were used: FTY-720 (Selleck, no. S5002), diABZI (Selleck, no. S8796), and RU.521 (Selleck, no. S6841).

Cytosolic dsDNA studies. The cytoplasm of organoids or MC38 tumor cells was extracted using a Mitochondria Isolation Kit (Thermo Fisher Scientific, no. 89874). Cytosolic dsDNA was quantified using the Quant-iT PicoGreen dsDNA Assay Kit (Thermo Fisher Scientific, no. P11496). For staining cytosolic dsDNA, PicoGreen (200-fold dilution) and MitoTracker (100 nM) (Thermo Fisher Scientific, no. M7512) were added to MC38 cell culture media for 1 h.

Tumor radioimmunotherapy. Male C57BL/6 mice were subcutaneously inoculated with 5×10^5 MC38 cells on the left flanks (primary tumor) on day 0 and the right flanks (secondary tumor) 3 d later. Ten days after implanting primary tumors, mice were subjected to RT with different radiation modalities for 5 Gy at a time for 5 consecutive days (5 Gy × 5). An anti-mouse PD-L1 monoclonal antibody (Bio X Cell; clone 10F.9G2, 10 mg/kg, i.p.) was injected into mice on day 10 after the primary tumor was implanted and was injected every 2 d for a total of four times.

Data, Materials, and Software Availability. All study data are included in the article and/or *SI Appendix*.

ACKNOWLEDGMENTS. We acknowledge State Key Laboratory of Radiation Medicine and Protection, Collaborative Innovation Center of Radiological Medicine of Jiangsu Higher Education Institutions, and Jiangsu Provincial Key Laboratory of Radiation Medicine for their support. We acknowledge Drs. Z. Chai, M. Gao, G. Zhou, Z. Shang, W. Yang, N. Liu, and W. Hu from the School of Radiation Medicine and Protection, Soochow University; Dr. Y. Zhang from the School of Biomedical Engineering, Shanghai Jiao Tong University; and Dr. Hongyu Zhu from the Department of Radiation Oncology, Sun Yat-sen University Cancer Center, for their valuable and inspiring discussions. We acknowledge L. Shan, L. Chen, C. Lao, J. Liu, T. He, and Y. Xu from the Institute of Applied Electronics, China Academy of Engineering Physics, for their support during FLASH X-ray experiments. We acknowledge J. Wan, J. Nie, and J. Wang from Suzhou Medical College of Soochow University and L. Bai from the Department of Radiotherapy, West China Hospital, Sichuan University, for their support during CONV X-ray experiments. We acknowledge M. Zhang and Y. Wang from the Laboratory Animal Center of Soochow University, for their support during animal experiments. This work was supported by the National Natural Science Foundation of China (Grants 82173455 and 81602793 [to H.Z.], Grant 82101848 [to W.Z.], Grant 12005211 [to Z.Z.], Grant 11975218 [to D.W.], Grant 11805192 [to K.Z.], Grant 31770912 [to F.L.], and Grant 81771949 [to Z.W]), the Natural Science Key Fund for Colleges and Universities of Jiangsu Province of China (Grant 21KJA310001 [to H.Z.]), and the Opening Foundation of State Key Laboratory of Radiation Medicine and Protection (Grant GZK1202122 [to H.Z.]).

Author affiliations: [a]School of Radiation Medicine and Protection, Suzhou Medical College of Soochow University, Suzhou 215123, China; [b]Institute of Applied Electronics, China Academy of Engineering Physics, Mianyang 621900, China; [c]Jiangsu Key Laboratory of Infection and Immunity, Institutes of Biology and Medical Sciences, Soochow University, Suzhou 215123, China; [d]Graduate School of China Academy of Engineering Physics, Beijing 100088, China; [e]Department of Oncology, Nuclear Medicine Laboratory of Mianyang Central Hospital, School of Medicine, University of Electronic Science and Technology of China, Mianyang 621000, China; [f]National Health Commission Key Laboratory of Nuclear Technology Medical Transformation, Mianyang Central Hospital, Mianyang 621000, China; [g]Department of Radiotherapy, State Key Laboratory of Biotherapy and Cancer Center, West China Hospital, Sichuan University, Chengdu 610041, China; [h]Department of Interventional Radiology, Ruijin Hospital, Shanghai Jiao Tong University School of Medicine, Shanghai 200025, China; and [i]Institute of Radiation Medicine, Fudan University, Shanghai 200032, China

1. A. Ribas, J. D. Wolchok, Cancer immunotherapy using checkpoint blockade. *Science* **359**, 1350–1355 (2018).
2. S. L. Topalian *et al.*, Immunotherapy: The path to win the war on cancer? *Cell* **161**, 185–186 (2015).
3. L. Galluzzi, T. A. Chan, G. Kroemer, J. D. Wolchok, A. López-Soto, The hallmarks of successful anticancer immunotherapy. *Sci. Transl. Med.* **10**, eaat7807 (2018).
4. S. Upadhaya *et al.*, Combinations take centre stage in PD1/PDL1 inhibitor clinical trials. *Nat. Rev. Drug Discov.* **20**, 168–169 (2021).
5. R. M. Chabanon *et al.*, Targeting the DNA damage response in immuno-oncology: Developments and opportunities. *Nat. Rev. Cancer* **21**, 701–717 (2021).
6. S. Demaria, C. N. Coleman, S. C. Formenti, Radiotherapy: Changing the game in immunotherapy. *Trends Cancer* **2**, 286–294 (2016).
7. S. P. Pitroda, S. J. Chmura, R. R. Weichselbaum, Integration of radiotherapy and immunotherapy for treatment of oligometastases. *Lancet Oncol.* **20**, e434–e442 (2019).
8. E. Deutsch, C. Chargari, L. Galluzzi, G. Kroemer, Optimising efficacy and reducing toxicity of anticancer radioimmunotherapy. *Lancet Oncol.* **20**, e452–e463 (2019).
9. S. C. Formenti *et al.*, Radiotherapy induces responses of lung cancer to CTLA-4 blockade. *Nat. Med.* **24**, 1845–1851 (2018).
10. K. W. Mouw, M. S. Goldberg, P. A. Konstantinopoulos, A. D. D'Andrea, DNA damage and repair biomarkers of immunotherapy response. *Cancer Discov.* **7**, 675–693 (2017).
11. T. Reisländer, F. J. Groelly, M. Tarsounas, DNA damage and cancer immunotherapy: A STING in the tale. *Mol. Cell* **80**, 21–28 (2020).
12. F. Meric-Bernstam, J. Larkin, J. Tabernero, C. Bonini, Enhancing anti-tumour efficacy with immunotherapy combinations. *Lancet* **397**, 1010–1022 (2021).
13. X. Zhou *et al.*, Treatment-related adverse events of PD-1 and PD-L1 inhibitor-based combination therapies in clinical trials: A systematic review and meta-analysis. *Lancet Oncol.* **22**, 1265–1274 (2021).
14. A. C. Tree *et al.*, Dose-limiting urinary toxicity with pembrolizumab combined with weekly hypofractionated radiation therapy in bladder cancer. *Int. J. Radiat. Oncol. Biol. Phys.* **101**, 1168–1171 (2018).
15. M. A. Postow, R. Sidlow, M. D. Hellmann, Immune-related adverse events associated with immune checkpoint blockade. *N. Engl. J. Med.* **378**, 158–168 (2018).
16. V. Favaudon *et al.*, Ultrahigh dose-rate FLASH irradiation increases the differential response between normal and tumor tissue in mice. *Sci. Transl. Med.* **6**, 245ra93 (2014).
17. B. Lin *et al.*, FLASH radiotherapy: History and future. *Front. Oncol.* **11**, 644400 (2021).
18. C. Fouillade *et al.*, FLASH irradiation spares lung progenitor cells and limits the incidence of radio-induced senescence. *Clin. Cancer Res.* **26**, 1497–1506 (2020).
19. B. Hu *et al.*, The DNA-sensing AIM2 inflammasome controls radiation-induced cell death and tissue injury. *Science* **354**, 765–768 (2016).
20. P. Broz, P. Pelegrín, F. Shao, The gasdermins, a protein family executing cell death and inflammation. *Nat. Rev. Immunol.* **20**, 143–157 (2020).
21. J. Shi *et al.*, Cleavage of GSDMD by inflammatory caspases determines pyroptotic cell death. *Nature* **526**, 660–665 (2015).
22. Y. Wang *et al.*, Chemotherapy drugs induce pyroptosis through caspase-3 cleavage of a gasdermin. *Nature* **547**, 99–103 (2017).
23. Z. Zhou *et al.*, Granzyme A from cytotoxic lymphocytes cleaves GSDMB to trigger pyroptosis in target cells. *Science* **368**, eaaz7548 (2020).
24. Z. Zhang *et al.*, Gasdermin E suppresses tumour growth by activating anti-tumour immunity. *Nature* **579**, 415–420 (2020).

25. P. Montay-Gruel *et al.*, Hypofractionated FLASH-RT as an effective treatment against glioblastoma that reduces neurocognitive side effects in mice. *Clin. Cancer Res.* **27**, 775–784 (2021).
26. P. Montay-Gruel *et al.*, Long-term neurocognitive benefits of FLASH radiotherapy driven by reduced reactive oxygen species. *Proc. Natl. Acad. Sci. U.S.A.* **116**, 10943–10951 (2019).
27. J. L. Ruan *et al.*, Irradiation at ultra-high (FLASH) dose rates reduces acute normal tissue toxicity in the mouse gastrointestinal system. *Int. J. Radiat. Oncol. Biol. Phys.* **111**, 1250–1261 (2021).
28. H. Dong, G. Zhu, K. Tamada, L. Chen, B7-H1, a third member of the B7 family, co-stimulates T-cell proliferation and interleukin-10 secretion. *Nat. Med.* **5**, 1365–1369 (1999).
29. G. Morad, B. A. Helmink, P. Sharma, J. A. Wargo, Hallmarks of response, resistance, and toxicity to immune checkpoint blockade. *Cell* **184**, 5309–5337 (2021).
30. E. Soularue *et al.*, Enterocolitis due to immune checkpoint inhibitors: A systematic review. *Gut* **67**, 2056–2067 (2018).
31. M. Hauer-Jensen, J. W. Denham, H. J. Andreyev, Radiation enteropathy–pathogenesis, treatment and prevention. *Nat. Rev. Gastroenterol. Hepatol.* **11**, 470–479 (2014).
32. T. Evans, J. Cooley, M. Wagner, T. Yu, T. Zwart, Demonstration of the FLASH effect within the spread-out Bragg peak after abdominal irradiation of mice. *Int. J. Part. Ther.* **8**, 68–75 (2021).
33. H. Zhu *et al.*, Radioprotective effect of X-ray abdominal FLASH irradiation: Adaptation to oxidative damage and inflammatory response may be benefiting factors. *Med. Phys.* **49**, 4812–4822 (2022).
34. A. Ayyaz *et al.*, Single-cell transcriptomes of the regenerating intestine reveal a revival stem cell. *Nature* **569**, 121–125 (2019).
35. S. J. Dovedi *et al.*, Fractionated radiation therapy stimulates antitumor immunity mediated by both resident and infiltrating polyclonal T-cell populations when combined with PD-1 blockade. *Clin. Cancer Res.* **23**, 5514–5526 (2017).
36. J. Wei *et al.*, Sequence of αPD-1 relative to local tumor irradiation determines the induction of abscopal antitumor immune responses. *Sci. Immunol.* **6**, eabg0117 (2021).
37. G. Kroemer, L. Galluzzi, O. Kepp, L. Zitvogel, Immunogenic cell death in cancer therapy. *Annu. Rev. Immunol.* **31**, 51–72 (2013).
38. D. Dangaj *et al.*, Cooperation between constitutive and inducible chemokines enables T cell engraftment and immune attack in solid tumors. *Cancer Cell* **35**, 885–900.e10 (2019).
39. J. M. Romero *et al.*, A four-chemokine signature is associated with a T-cell-inflamed phenotype in primary and metastatic pancreatic cancer. *Clin. Cancer Res.* **26**, 1997–2010 (2020).
40. L. Jia, W. Zhang, C. Y. Wang, BMI1 inhibition eliminates residual cancer stem cells after PD1 blockade and activates antitumor immunity to prevent metastasis and relapse. *Cell Stem Cell* **27**, 238–253.e6 (2020).
41. J. W. Schoggins *et al.*, A diverse range of gene products are effectors of the type I interferon antiviral response. *Nature* **472**, 481–485 (2011).
42. J. M. Ramanjulu *et al.*, Design of amidobenzimidazole STING receptor agonists with systemic activity. *Nature* **564**, 439–443 (2018).
43. C. Vanpouille-Box *et al.*, DNA exonuclease Trex1 regulates radiotherapy-induced tumour immunogenicity. *Nat. Commun.* **8**, 15618 (2017).
44. K. Levy *et al.*, Abdominal FLASH irradiation reduces radiation-induced gastrointestinal toxicity for the treatment of ovarian cancer in mice. *Sci. Rep.* **10**, 21600 (2020).
45. J. T. Eggold *et al.*, Abdominopelvic FLASH irradiation improves PD-1 immune checkpoint inhibition in preclinical models of ovarian cancer. *Mol. Cancer Ther.* **21**, 371–381 (2022).
46. F. Gao *et al.*, First demonstration of the FLASH effect with ultrahigh dose rate high-energy X-rays. *Radiother. Oncol.* **166**, 44–50 (2022).
47. H. Nishimura, T. Honjo, PD-1: An inhibitory immunoreceptor involved in peripheral tolerance. *Trends Immunol.* **22**, 265–268 (2001).
48. B. T. Fife, J. A. Bluestone, Control of peripheral T-cell tolerance and autoimmunity via the CTLA-4 and PD-1 pathways. *Immunol. Rev.* **224**, 166–182 (2008).
49. M. Mestres, M. R. Caballín, L. Barrios, M. Ribas, J. F. Barquinero, RBE of X rays of different energies: A cytogenetic evaluation by FISH. *Radiat. Res.* **170**, 93–100 (2008).
50. X. Cao *et al.*, Quantification of oxygen depletion during FLASH irradiation in vitro and in vivo. *Int. J. Radiat. Oncol. Biol. Phys.* **111**, 240–248 (2021).
51. D. Hanahan, R. A. Weinberg, Hallmarks of cancer: The next generation. *Cell* **144**, 646–674 (2011).
52. D. Hanahan, Hallmarks of cancer: New dimensions. *Cancer Discov.* **12**, 31–46 (2022).